Supporting Information

Chemical Rescue of Enzymes: Proton Transfer in Mutants of Human Carbonic Anhydrase II

C. Mark Maupin[†], Norberto Castillo[†], Srabani Taraphder[†,‡], Chingkuang Tu[§], Robert McKenna[,‖], David N. Silverman[*,§,‖], and Gregory A. Voth[*,†,⊥]*

Center for Biophysical Modeling and Simulation and Department of Chemistry, University of Utah, Salt Lake City, UT 84112.

Department of Chemistry, Indian Institute of Technology, Kharagpur 721302, India

Department of Pharmacology and Therapeutics,

Department of Biochemistry and Molecular Biology

University of Florida, Gainesville, FL 32610

Department of Chemistry, James Frank Institute, and Computation Institute

University of Chicago, 5735 S. Ellis Ave., Chicago, IL 60637

[†]Center for Biophysical Modeling and Simulation and the Department of Chemistry, University of Utah.

[‡]Department of Chemistry, Indian Institute of Technology, Kharagpur 721302, India

[§]Department of Pharmacology and Therapeutics, University of Florida.

[‖]Department of Biochemistry and Molecular Biology, University of Florida.

[⊥]Department of Chemistry, University of Chicago

[*]Corresponding authors: Gregory A. Voth, email: gavoth@uchicago.edu; David N. Silverman, email: silvrmn@ufl.edu; Robert McKenna, email: rmckenna@ufl.edu.

Ref 61.

Case, D. A.; Darden, T. A.; Cheatham III, T. E.; Simmerling, C. L.; Wang, J.; Duke, R. R.; Luo, R.; Crowley, M.; Walker, R. C.; Zhang, W.; Merz, K. M.; Wang, B.; S. Hayik, A.; Roitberg, G.; Seabra, I.; Kolossvary; Wong, K. F.; Paesani, F.; Vanicek, J.; Wu, X.; Brozell, S. R.; Steinbrecher, T.; Gohlke, H.; Yang, L.; Tan, C.; Mongan, J.; Horn, V.; Cui, G.; Mathews, D. H.; Seetin, M. G.; Sagui, C.; Babin, V.; Kollman, P. A.; Amber 10th ed.; University of California: San Francisco, 2008.

Table 1S. MS-EVB parameters for 4MI

V^0_{ii}	-105.106 kcal mol^{-1}
V_{ij}^{const}	-96.92 kcal mol^{-1}
$r_{sc}^{\ 0}$	1.19 Å
λ	0.06
$R_{DA}^{\ 0}$	2.47 Å
C	0.46
a	1.33 Å^{-2}
a_{DA}	3.72 Å^{-2}
β	3.50 Å^{-2}
b_{DA}	2.20 Å
ε	13.54 Å^{-1}
C_{DA}	2.25 Å
γ	2.27 Å^{-2}

MS-EVB Simulations of 4MI. The AMBER10 and MS-EVB2 systems for the 4MI simulations were created by solvating the $4MIH^+$ molecule in a box of 1009 modified TIP3P[1] water molecules (box dimensions of 30.8 Å x 30.8 Å x 33.1 Å) and a chloride counter ion. The solvated system was then relaxed for 4000 steps using the steepest descent method followed by a pre-equilibration MD run of 250 ps in the constant NPT ensemble using the AMBER10 package.[2,3] The constant NPT simulations were conducted at 298.15 K and used periodic boundary conditions with long-range Coulombic interactions calculated by Ewald summation.[4] The MD time integration step was 1 fs and used the leapfrog Verlet integrator while the short-ranged nonbonded interactions and forces were subject to a 10 Å cutoff. The simulation was run at 1 atm and utilized Langevin dynamics for the thermostat. The pre-equilibrated system was then transferred to a modified DL-POLY 2.15 software package[5] incorporating the MS-EVB2 algorithm and equilibrated for 250 ps in the constant NVT ensemble to allow the system to adjust to the presence of the delocalized hydrated proton charge defect. The PMF calculations for the deprotonation event consisted of 32 umbrella sampling windows spanning the range of ξ_0^n = 0.8-7 Å , where ξ_0^n is defined as the distance between the delta nitrogen (N_δ) of 4MI and the excess proton CEC. An umbrella potential with a force constant of k_n = 40 kcal mol^{-1} $Å^{-2}$ was used to restrain the CEC to ensure adequate sampling along the reaction coordinate. Each window was equilibrated in the constant NVT ensemble for 200 ps followed by a data collection period of 1 ns to 2 ns depending on convergence of the window. All MS-EVB simulations were run at 300 K, used a Nosé-Hoover thermostat, periodic boundary conditions with long-range Columbic interactions calculated by the Ewald summation, a 9.5 Å cutoff for the short-ranged nonbonded interactions and a Verlet integrator step of 1fs. The weighted histogram analysis method[6,7] (WHAM) was used to match the umbrella sampling windows together to form a

continuous PMF. The error in the PMFs was calculated using the Monte Carlo bootstrap error analysis method. The resulting PMF for the deprotonation of 4MI can be found in the Figure 1S.

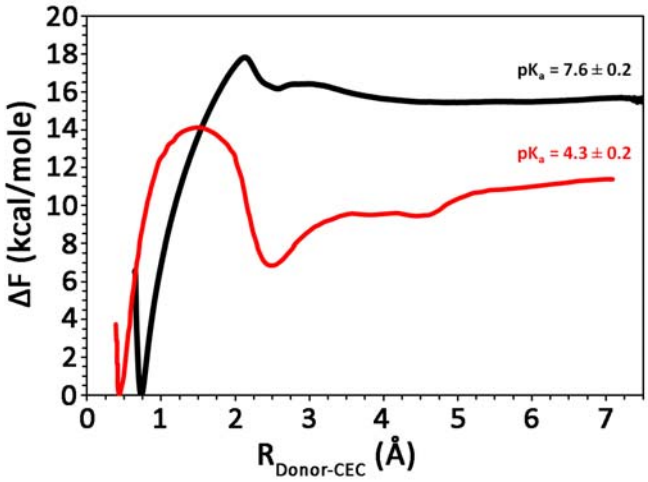

Figure 1S. Free energy profile for the amino acid deprotonation reaction for 4MI (black) and glutamate (red). The glutamate model is a modification of the model reported in ref 50 (V_{ii}^0 value of -109.72 kcal/mol all other parameters are unchanged). The thickness of the line denotes the standard deviation, which was evaluated to be ≤ 0.2 kcal/mol.

Equilibration Analysis. The H64A-HCA II mutant systems, with and without 4MI, possess RMSD plots similar to those shown in Figure 2S. Typical of the HCA II systems, the RMSD quickly plateaued to a value around 1 Å within the first 300 ps of the equilibration run (equilibration run was conducted after the initial 100 ps annealing simulations from 0 K to 300 K). In addition to the RMSD plot the total and potential energy for the equilibration simulations was analyzed. It is clear from Figure 3S that the energy components of the system are stable. The RMSD and energy plots indicate that the equilibration protocol outlined in this manuscript is sufficient in length to adequately bring the system to equilibrium.

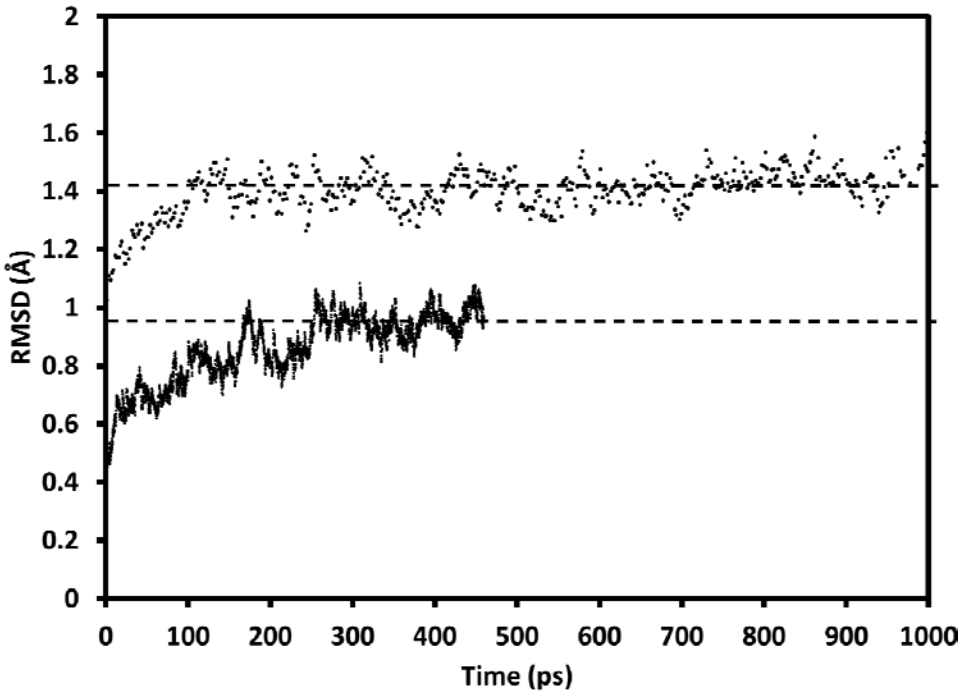

Figure 2S: Representative RMSD plot for the H64A systems during the equilibration phase (bottom curve) and a longer simulation including the data collection phase (upper curve). The upper curve is shifted up by 0.5 Å for clarity and a dotted line is added to each curve for comparison to linearity. The black line (bottom curve) was taken from the equilibration of H64A HCA II system with 4MI in the secondary x-ray binding site. The dotted black line (upper curve) was taken from the equilibration and portion of the production phase for the H64A HCA II system without 4MI present.

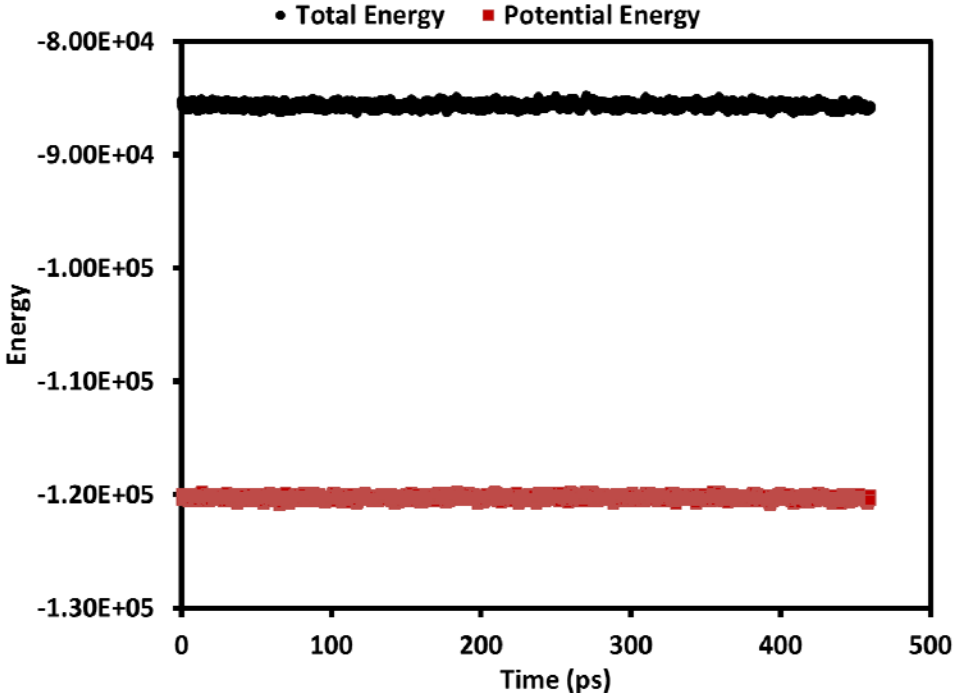

Figure 3S: Representative energy component plot for the H64A systems during the equilibration phase.

MS-EVB Simulations of Self-Rescue by Glu69. Figure 4S represents the various PT pathways explored in this manuscript. The red solid line shows the self-rescue pathway utilizing Glu69. From Figure 4S it is clear that the Glu69 slightly stabilize the intramolecular water wire, lowering the free energy by ~ 2 kcal/mol. This stabilization of the intramolecular water wire is also seen the RDF for the active site waters (Figure 5S). The modest decrease in the free energy barrier is not enough to account for observed rate in the H64A mutant in the absence of chemical rescue agents. The slight decrease in the free energy barrier is accompanied by an increasing stabilization of the excess proton as it moves closer to the position of Glu69 (as compared to the black solid line). Beyond the grey dash-dotted line (~ 12 Å) the error in the PMF grows significantly, indicating that the distal portion of the PMF is unconverged. The PMF was not

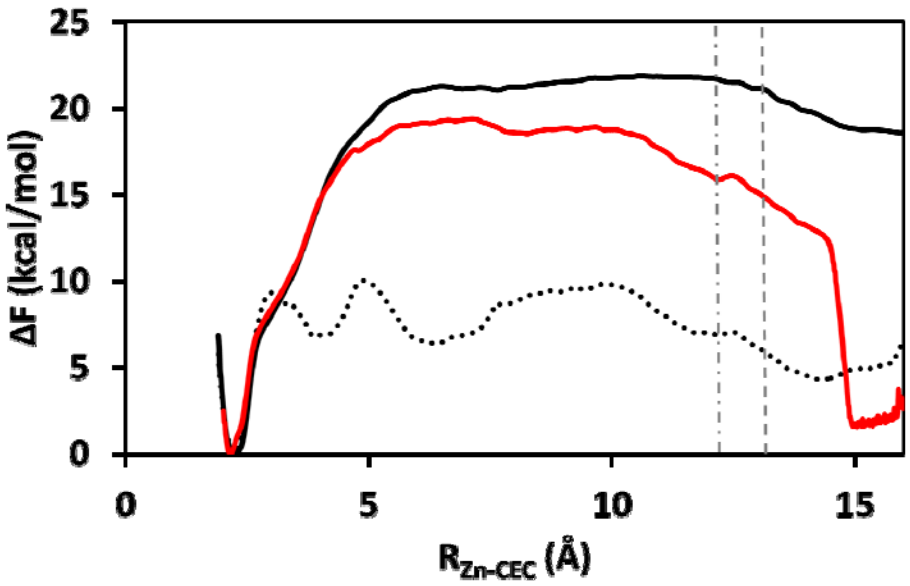

Figure 4S: PMF estimate for self-rescue of the H64A mutant by Glu69. The black solid line indicates the data for the PT PMF in the H64A II mutant without 4MI and not exploring self-rescue by Glu69. The black dotted line indicates the chemical rescue by 4MI in the NMR binding site and the subsequent PT to Glu69. The red solid line indicates the self-rescue by Glu69. The grey dashed-dotted line indicates when the error surpassed 0.5 kcal/mol and the dashed line indicates the point at which the error grows larger than 1 kcal/mol (error is from the unconverged distal portion of the red line only).

fully converged in this distal region (≥ 13 Å) due to the converged portion of the free energy barrier (~ 5 Å) indicating that this pathway is not productive. The general trend of the distal region of the PMF indicates that the free energy continues to decrease and that there is evidence of a stabilized $GluH^+$ at ~ 15 Å.

4MI Binding at the X-ray Binding Sites. The viability of the 4MI chemical rescue moiety depends on many factors including the impact of 4MI on the intramolecular water cluster, distance from the catalytic zinc, pK_a of the ionizable residue, and formation of hydrogen bonding networks conducive to proton transport. The impact of 4MI on the intramolecular water cluster is found in Figure 5S. As discussed in the manuscript the presence of 4MI in either x-ray binding site has an impact on the intramolecular water cluster. Clearly the presence of 4MI lowers the amplitude of the first peak (W1) bringing it more in line with the WT system. While the

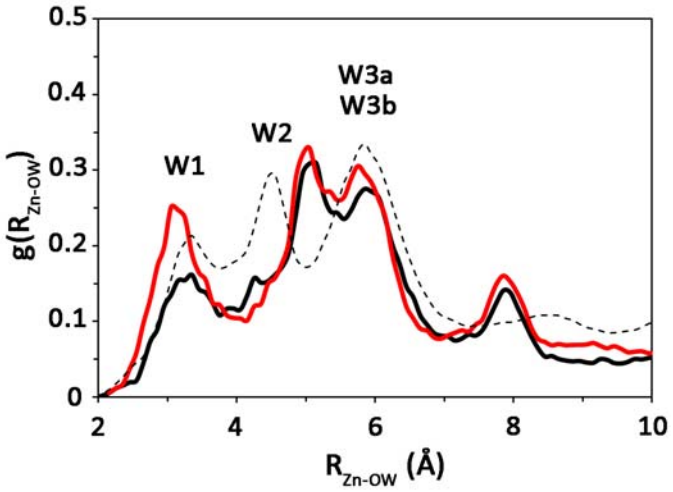

Figure 5S. Radial distribution function of the active site waters for H64A HCA II with 4MI bound near Trp5 (black) and Glu69 (red). For reference purposes the WT ZnH_2O^{2+} system with His64 in the outward orientation is included (black dotted).[16]

amplitude of the first peak becomes more similar to the WT the second peak is shifted (compared to H64A without 4MI) to larger distances. This may be due to an increased hydrogen bonding

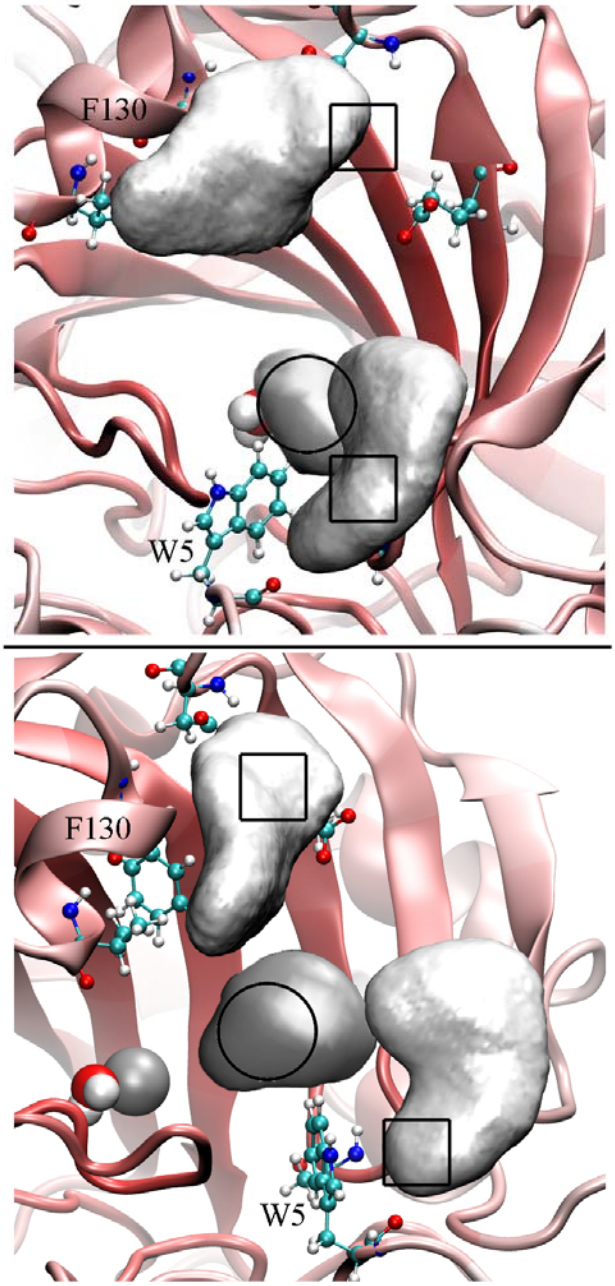

Figure 6S: Spatial occupancy plots of the 4MI molecule associating with H64A HCA II. The squares indicate the 4MI binding sites determined from x-ray (lighter iso-surfaces) and the circle indicates the binding site determined from NMR data (dark iso-surface). The gray regions represent the 75% occupancy iso-surface.

environment around the 4MI molecule. On close inspection it is seen that the first minimum in Figure 5S is at a higher value than that for H64A in the absence of 4MI (~ 4Å in Figure 3). This would indicate the presence of waters (due to the increased amplitude), but also an increase in the waters mobility (i.e., a stable water will have a well-defined peak and troughs while mobile water will result in a relatively flat distribution with an amplitude indicative of the amount of water present). Therefore, the RDFs indicate that while the presence of 4MI stabilized some waters it results in a reduced order of waters in the critical region around 4 Å. This region corresponds to the typical location of W2 the branching point in the water cluster that connects the bound water to the surrounding solution. The disruption of water orientation in this region has been implicated in a reduced ability to transport an excess proton.[8]

In addition to the impact of 4MI on the surrounding water environment it is also important to identify the location and relative association of 4MI with the H64A HCA II mutant. Figure 6S depicts the occupancy plot for 4MI binding/association over the 3 ns trajectories as outlined in the manuscript. The occupancy data reveals that 4MI weakly associates at both of the x-ray binding sites. The relatively large occupancy iso-surface reveals that 4MI is mobile at both sites freely associating at several locations near the x-ray binding sites. As the iso-surface encompasses more density (reduced iso-surface value) the 4MI is seen to increase the volume that it samples to the point where all the densities overlap and a general picture of the 4MI weakly associating around the mouth of the enzyme becomes evident.

Analysis of the hydrogen bonding networks from the zinc bound water to the 4MI molecule in either x-ray binding site resulted in larger water clusters (due to the increased separation distance) and very low probabilities (due in part to 4MI's mobility and the increased mobility of W2 and W3b). Figure 7S depicts the water cluster characteristics of the H64A HCA II mutant in the presence of 4MI associating in either x-ray determined binding sites. The water cluster analysis reveals that although 4MI is associating with the H64A mutant enzyme these systems are incapable of forming stable water clusters similar to the WT systems with His64 in either the inward or outward orientation. The water cluster distribution for the primary x-ray binding site is similar in shape to that of the WT system with His64 in the outward orientation

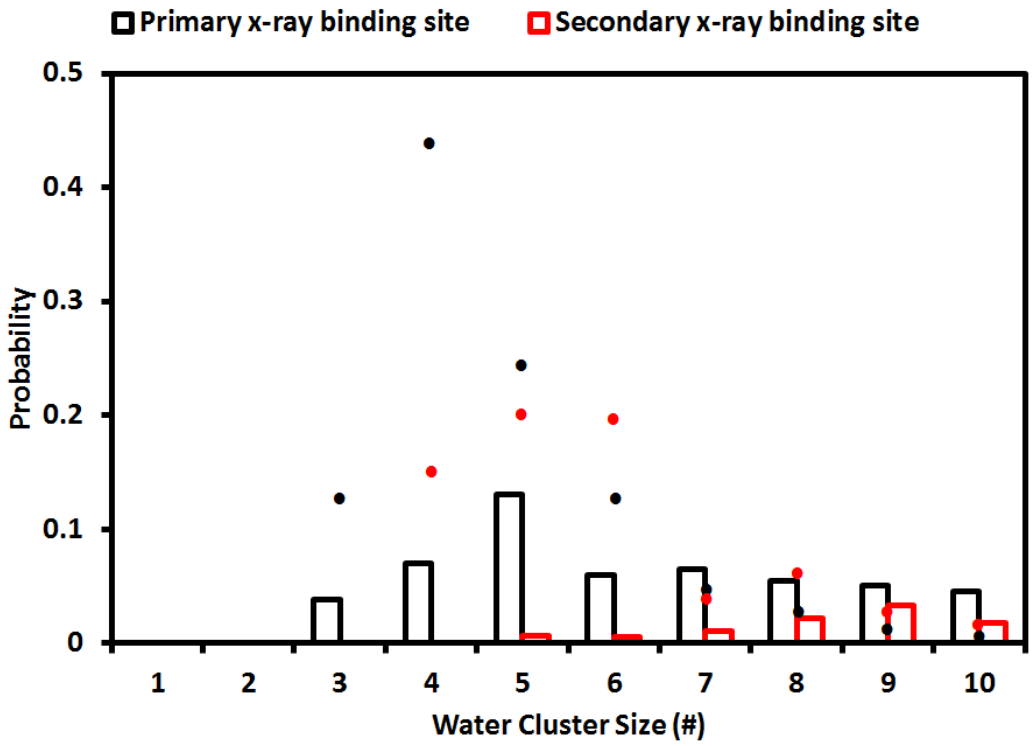

Figure 7S: Water cluster distribution for 4MI associating with the H64A HCA II mutant. The primary binding site is near Trp5 and the secondary binding site is near Glu69. For comparison the WT ZnH_2O His64 in the in orientation (small black circle) and the WT ZnH_2O His64 in the out orientation (small red circle) are included.

although the probabilities for the 4MI system are significantly smaller. The presence of a size 3 water cluster is due to the mobility of the 4MI molecule and is more accurately described by the 4MI occupying the NMR binding site. The water cluster distribution for the secondary binding site is shifted to larger cluster sizes due to the fact that this binding site is farther away than the primary binding site. In addition, the probability of forming water clusters is greatly reduced when compared to the primary binding site. These results indicate that the formation of water clusters conducive to proton transport is a rare event.

In addition to the above analysis the underlying PMF for proton transport in the H64A HCA II mutant and the deprotonation PMFs for 4MI and Glu are compared, Figure 8S. The discussion in this section is also extended to include the possibility of self-rescue by Glu69, due to the similar use of interaction distances. An important concept in this PMF collage is the interaction distance for 4MI and Glu. The interaction distance is the furthest distance that an excess proton interacts with the ionizable moiety. From Figure 8S it is clear that Glu has a much larger interaction distance than 4MI. Placing the PMF for 4MI at 10 Å, similar to the position of 4MI bound to the primary x-ray determined binding site, it is clear that the short interaction distance of 4MI makes it improbable that 4MI at this distance could significantly lower the PMF. Even in an ideal situation, assuming 4MI acts identical to His64 in the outward orientation in the WT system, we would estimate a free energy barrier of around 11 kcal/mol.[9] Yet, it is clear from the occupancy data, RDF, and water cluster information that this is not an ideal situation. Therefore the free energy barrier for proton transport would be estimated to higher than 11 kcal/mol. Making this binding site a non-viable candidate for chemical rescue. Along the same lines of reasoning the secondary x-ray binding site for 4MI and the self-rescue pathway utilizing Glu69 may be eliminated.

The weak association of the 4MI molecule with the x-ray binding sites, the inability of the 4MI in these locations to stabilize waters in the 4 Å region, the small probability of forming stabilizing hydrogen bonded water clusters connecting the proton donor/acceptor pair, and the unfavorable PMF estimate results strongly indicates that these binding sites are non-productive. That is to say, the free energy resulting from using these pathways would be higher than using an alternate, as of yet unidentified, pathway. When all the characteristics for the viability of 4MI in either x-ray binding site are taken together it is concluded that 4MI in either of these binding sites is non-productive.

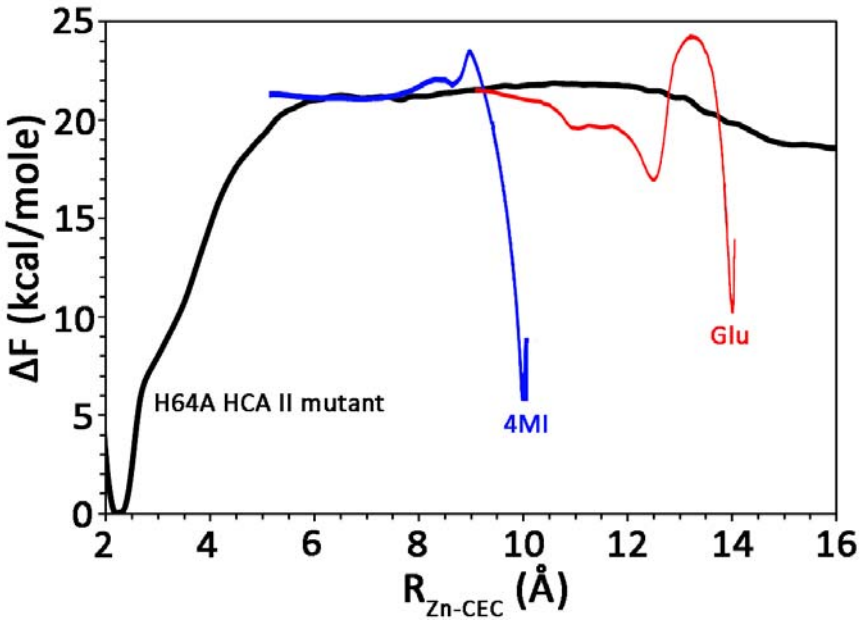

Figure 8S: PMF estimates for chemical rescue by 4MI at the x-ray determined binding sites and self-rescue by Glu69. The black line depicts proton transport in the H64A HCA II mutant without 4MI. The blue line represents the deprotonatation PMF for 4MI positioned near the primary x-ray binding site. The red line represents the Glu deprotonation PMF for Glu69.

References.

(1) Day, T. J.; Soudackov, A. V.; Cuma, M.; Schmitt, U. W.; Voth, G. A. *J. Chem. Phys.* **2002**, *117*, 5839.

(2) Wang, J.; Cieplak, P.; Kollman, P. A. *J. Comput. Chem.* **2000**, *21*, 1049.

(3) Case, D. A.; Darden, T. A.; Cheatham III, T. E.; Simmerling, C. L.; Wang, J.; Duke, R. R.; Luo, R.; Crowley, M.; Walker, R. C.; Zhang, W.; Merz, K. M.; Wang, B.; S. Hayik, A.; Roitberg, G.; Seabra, I.; Kolossvary; Wong, K. F.; Paesani, F.; Vanicek, J.; Wu, X.; Brozell, S. R.; Steinbrecher, T.; Gohlke, H.; Yang, L.; Tan, C.; Mongan, J.; Horn, V.; Cui, G.; Mathews, D. H.; Seetin, M. G.; Sagui, C.; Babin, V.; Kollman, P. A.; Amber 10th ed.; University of California: San Francisco, 2008.

(4) Hummer, G.; Pratt, L. R.; Garcia, A. E. *J. Phys. Chem* **1996**, *100*, 1206.

(5) Smith, W.; Forester, T. R.; CCLRC, Daresbury Laboratory: Daresbury, Warrington, England, 1999.

(6) Kumar, S.; Bouzida, D.; Swendsen, R. H.; Kollman, P. A.; Rosenberg, J. M. *J. Comp. Chem.* **1992**, *13*, 1011.

(7) Roux, B. *Comput. Phys. Commun.* **1995**, *91*, 275.

(8) Maupin, C. M.; Zheng, J.; Tu, C.; McKenna, R.; Silverman, D. N.; Voth, G. A. *Biochemistry* **2009**, *48*, 7996.

(9) Maupin, C. M.; McKenna, R.; Silverman, D. N.; Voth, G. A. *J. Am. Chem. Soc.* **2009**, *131*, 7598.